Wind and Structures, *Vol. 26, No. 4 (2018) 191-204*
DOI: https://doi.org/10.12989/was.2018.26.4.191

Study of random characteristics of fluctuating wind loads on ultra-large cooling towers in full construction process

S.T. Ke[*1,2], L. Xu[1] and Y.J. Ge[2]

[1]*Department of Civil Engineering, Nanjing University of Aeronautics and Astronautics, 29 Yudao Road, Nanjing 210016, China*
[2]*State Key Laboratory for Disaster Reduction in Civil Engineering, Tongji University, 1239 Siping Road, Shanghai 200092, China*

(Received September 14, 2017, Revised January 12, 2018, Accepted January 27, 2018)

Abstract. This article presents a study of the largest-ever (height = 220 m) cooling tower using the large eddy simulation (LES) method. Information about fluid fields around the tower and 3D aerodynamic time history in full construction process were obtained, and the wind pressure distribution along the entire tower predicted by the developed model was compared with standard curves and measured curves to validate the effectiveness of the simulating method. Based on that, average wind pressure distribution and characteristics of fluid fields in the construction process of ultra-large cooling tower were investigated. The characteristics of fluid fields in full construction process and their working principles were investigated based on wind speeds and vorticities under different construction conditions. Then, time domain characteristics of ultra-large cooling towers in full construction process, including fluctuating wind loads, extreme wind loads, lift and drag coefficients, and relationship of measuring points, were studied and fitting formula of extreme wind load as a function of height was developed based on the nonlinear least square method. Additionally, the frequency domain characteristics of wind loads on the constructing tower, including wind pressure power spectrum at typical measuring points, lift and drag power spectrum, circumferential correlations between typical measuring points, and vertical correlations of lift coefficient and drag coefficient, were analyzed. The results revealed that the random characteristics of fluctuating wind loads, as well as corresponding extreme wind pressure and power spectra curves, varied significantly and in real time with the height of the constructing tower. This study provides references for design of wind loads during construction period of ultra-large cooling towers.

Keywords: ultra-large cooling tower; full construction process; large eddy simulation; fluid field principles; time domain characteristics; frequency domain characteristics; extreme wind pressures

1. Introduction

Ultra-large cooling towers are tall core-shell structures readily exposed to wind loads. Currently, the size of cooling tower has increased continuously, resulting in increased effects of 3D dynamic wind loadings on the tower surface and elongated construction period. Especially, the mechanical performance of constructing structures varies in real time as the strength and elastic surface varied in the construction process. Owing to complicated effects of various factors in the construction process, few comprehensive studies of wind loads on the ultra-large cooling towers in full construction process have been reported. Therefore, designs of extreme load capacity in the construction process are extremely challenging.

Previous studies of wind loads on ultra-large cooling towers focused on average wind pressure distribution (Zhang *et al.* 2017) and fluctuating wind pressure distribution (Niemann and Pröpper 1975, Zahlten and Borri 1998) of constructed towers, as well as correlation effects of wind loads(Orlando 2001, Karakas *et al.* 2016)and wind-induced responses (Ke *et al*. 2014, Glanville and Kwok 1995)in multi-tower cases. Recently, non-Gaussian (Ke *et al*. 2015, Binh *et al.* 2008), instable (Ke *et al.* 2015, Mang *et al*. 2014), and extreme distributions of fluctuating wind pressures of ultra-large cooling towers (Dauhut *et al.* 2015) have been intensively studied. Ke *et al.* discussed determination of cross section volumetric coefficients and lift/drag correlation coefficients based on time history of wind pressure at measuring points obtained by wind tunnel tests and proposed a method for extreme value calculation (Ke *et al.* 2015). Li *et al.* investigated the distribution of circumferential stress section drag coefficients along the tower height based on distributions of fluctuating wind pressure on the tower surface obtained by wind tunnel tests and proposed fitting curves for circumferential distribution of extreme wind pressure, with correlations of different parameters taken into consideration (Li *et al*. 2008). Bao *et al.* studied natural frequency distribution and mode of cooling towers using the finite element method. Based on transient responses of cooling towers under fluctuating wind pressures, the time and frequency domains of cooling tower responses were obtained and the sampling interval in the autoregressive model of linear filtering was determined. Nevertheless, it is assured that the wind load distribution of cooling tower in the construction process were significantly different from the built cooling towers' (Bao *et al*. 2010).

*Corresponding author, Associate Professor
E-mail: keshitang@163.com
[a] Postgraduate
E-mail: luxunuaa@163.com
[b] Professor
E-mail: yaojunge@tongji.edu.cn

Copyright © 2018 Techno-Press, Ltd.

ISSN: 1226-6116 (Print), 1598-6225 (Online)

Table 1 Structural parameters under different construction conditions

	Condition A	Condition B	Condition C	Condition D	Condition E	Condition F
3D entity model			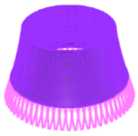			
Template layer	15	35	55	75	95	128
Height	50.90 m	80.07 m	109.60 m	139.43 m	169.41m	218.84 m
Min radius	78.00 m	71.00 m	65.73 m	62.54 m	61.67 m	61.67 m
Min thickness	0.51 m	0.49 m	0.45 m	0.38 m	0.38 m	0.38 m

Therefore, previous studies didn't involve average and fluctuating wind loads on towers under construction in full construction process and studies on time and frequency domains of wind loads on ultra-large cooling towers in full construction process are also absent.

In this article, high precision 3D entity models for different heights were established based on the largest-ever (height = 220 m) cooling tower. Information about fluid fields around the tower and 3D aerodynamic time history in full construction process were obtained using the large eddy simulation (LES) method. The average wind pressure distribution along the entire tower predicted by the developed model was compared with standard curves and measured curves to validate the effectiveness of the developed model. Based on that, average wind pressure distribution, characteristics of fluid fields in the construction process of ultra-large cooling tower, and the characteristics of fluid fields in full construction process, as well as their working principles, were investigated. On this basis, the fluctuating wind pressure, extreme wind pressure, overall lift and drag coefficient, power spectrum characteristics and correlation of typical measuring points in construction process is compared, and the rule of the influence of different construction height to the wind pressure is extracted. Based on the principle of nonlinear least square method, the fitting formula of extreme wind pressure was put forward.

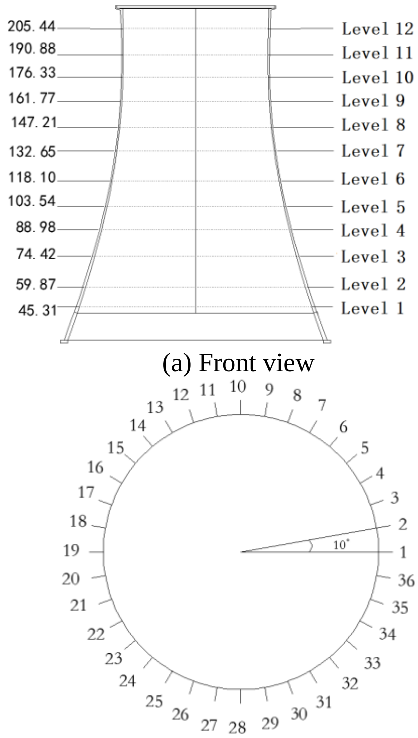

(a) Front view

(b) Top view

Fig. 1 Arrangement of measuring points on the cooling tower

2. Background

The ultra-large cooling tower located in the northwest of China (Level B landform) where the 50-year standard wind pressure is 0.35 kN/m^2 (corresponding wind speed = 23.7 m/s). The height of the cooling tower, the throat and the inlet are 220 m, 165 m, 30.75 m, respectively. The diameters of the top surface, neck section, and bottom surface are 128.1 m, 123 m, and 185 m, respectively. The wall thickness increased exponentially with the tower height (minimum thickness = 0.38 m, maximum thickness 1.85 m).

In order to investigate wind loads on ultra-large cooling towers in full construction process, six typical heights are defined. The existing references (Niemann *et al.* 2011, Ke *et al.* 2012) show that the existence of the end effect makes the distribution of the flow field at the junction between the tower tube and the pillar more special. In order to study the distribution of the flow field in the end, the first construction condition is set at the height of the 15-story formworks. The condition two to five are set every 20-story formworks. The condition 5, that is, the 95-story formwork is just near the throat, which can be used to study the weakest part of the tower. The condition six is the height of cooling tower. According to the tower template layers:

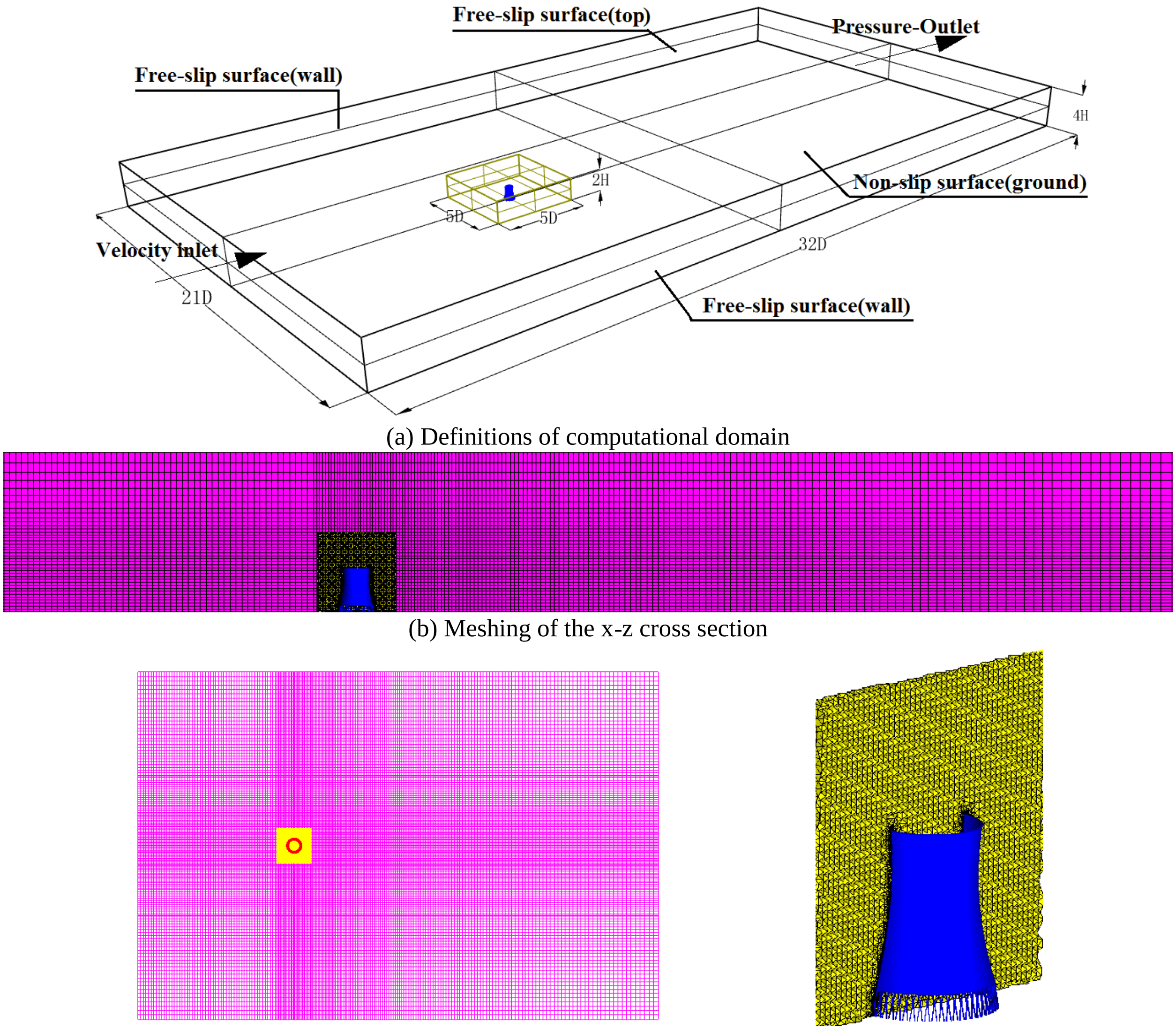

(a) Definitions of computational domain

(b) Meshing of the x-z cross section

(c) Vertical view

(d) Local encryption of the mesh

Fig. 2 The computational domain and mesh model diagram

construction conditions A = 15th template; construction conditions B = 35th template; construction conditions C = 55th template; construction conditions D = 75th template; construction conditions E = 95th template; construction conditions F = 128 templates. Parameters of all construction conditions and arrangement of measuring points are shown in Table 1 and Fig. 1, respectively.

3. Numerical simulation and validation

3.1 Computational domain and mesh generation

To guarantee full development of the wake, the computational domains were set as along-wind direction (32D), across-wind direction (21D), and vertical direction (4H). Herein, D and H are the bottom surface diameter and tower height, respectively. The distance from computation model center to computational domain entrance was 1800 m and the blocking probability was 1.5%. To optimize the calculation efficiency and accuracy, local areas near the tower surface were divided into non-structural meshes, while other areas were divided into structural meshes. The size of the grid increases from the inside to the outside. The minimum mesh size was 0.2 m, the overall mesh quantity was 17.5 million, and the grid quality was larger than 0.40 (>0.1 to avoid negative volume). Definitions of computational domains and mesh generation are shown in Fig. 2.

3.2 Governing equations of fluid mechanics

In the study of structural wind resistance, fluid is considered as viscous incompressible, and the transient N-S equation is spatially averaged. The governing equation of Large Eddy Simulation method is obtained

$$\frac{\partial \overline{\mu_i}}{\partial x_i} = 0 \tag{1}$$

$$\frac{\partial \overline{\mu_i}}{\partial t} + \frac{\partial (\overline{\mu_i}\,\overline{\mu_j})}{\partial x_j} = -\frac{1}{\rho}\frac{\partial \overline{p}}{\partial x_i} + v\frac{\partial^2 \overline{\mu_i}}{\partial x_j \partial x_j} - \frac{\partial \tau_{ij}}{\partial x_j} \tag{2}$$

In the above equations, ρ is the density of air, t is the time, v is the coefficient of viscosity in air motion. $\overline{\mu_i}$ and $\overline{\mu_j}$ represent the speed in the 3 directions after filtering; there, i and $j$equals1,2,3 respectively. x_i and x_j are three coordinate components of space respectively. $\overline{p}$ is the filtered pressure. τ_{ij} is the non-closed term of the N-S equation after space averaging, that is subgrid-scale stress.

$$\tau_{ij} = \overline{\mu_i \mu_i} - \overline{\mu_i}\,\overline{\mu_j} \tag{3}$$

According to the subgrid-scale model proposed by Smagorinsky based on the eddy viscosity assumption, the Boussinesq hypothesis is introduced. The subgrid-scale stress can be expressed as:

$$\tau_{ij} - \frac{1}{3}\tau_{ij}\delta_{ij} = -2\mu_t \overline{S_{ij}} = -\mu_t\left(\frac{\partial \overline{\mu_i}}{\partial x_j} + \frac{\partial \overline{\mu_j}}{\partial x_i}\right) \tag{4}$$

$\overline{S_{ij}}$ is the solvable scale strain rate tensor in the formula. δ_{ij} is the Kronecker delta function. μ_t is a subgrid-scale eddy viscosity, and the Smagorinsky assumption is generally used

$$\mu_t = (C_s \Delta)^2 \left|\overline{S}\right| \tag{5}$$

C_s is the Smagorinsky constant in the formula, and the range is 0.1~0.23,taking 0.1 in the text. The strain rate tensor $\left|\overline{S}\right|$ is equal to $\sqrt{2 S_{ij} S_{ij}}$. $\Delta = (\Delta_x \Delta_y \Delta_z)^{1/3}$ is the spatial grid scale, and Δ_x , Δ_y and Δ_z are mesh sizes of x, y, and z directions respectively. This is the standard Smagorinsky subgrid-scale model. Some researchers have proposed a method of dynamically determining the value to better consider the collision, separation, free shear layer and vortex shedding around the bluff body, andthis is called Dynamic Smagorinsky. Smagorinsky Model is a turbulent model for calculating high Reynolds number.

The basic idea of the Dynamic Smagorinsky model is to obtain information from the solved region through two different sub-scale strain rate tensors to solve the coefficients of the sub-grid scale model. These two different strain rate tensors are calculated by two different filter sizes (Main filter $\overline{\Delta}$ andsecondary filter $\hat{\overline{\Delta}}$, $\hat{\overline{\Delta}} > \overline{\Delta}$, usually take $\hat{\overline{\Delta}} = 2\overline{\Delta}$,). The amount of the following quadratic filtering is represented by “^” symbol. The subgrid stresses produced by two kinds of filters are τ_{ij}^{sgs} and T_{ij} respectively, and the relationship between them is

$$T_{\mathrm{ij}} - \tau_{ij}^{\mathrm{sgs}} = \widehat{\tilde{u}_i \tilde{u}_j} - \hat{\tilde{u}}_i \hat{\tilde{u}}_j = L_{ij} \tag{6}$$

The second order tensor $\boldsymbol{L}_{ij}$ is the stress generated by turbulent motion between the main filter $\overline{\Delta}$ and the secondary filter $\hat{\overline{\Delta}}$.For the Smagorinsky model, the subgrid stresses on these two scales are defined as

$$\tau_{ij}^{sgs} = 2\rho C_s \overline{\Delta}^2 \left|\overline{S}\right| \overline{S}_{ij} \ , \ T_{\mathrm{ij}} = 2\rho C_s \hat{\overline{\Delta}}^2 \left|\hat{\overline{S}}\right| \hat{\overline{S}}_{ij} \tag{7}$$

Where $\left|\overline{S}\right|$ is the modulus of the stress tensor ($\left|\overline{S}\right| = \sqrt{2\overline{S}_{ij}\overline{S}_{ij}}$).

So the two - order tensor $\boldsymbol{L}_{ij}$ is changed to

$$L_{ij} = 2\rho C_s \hat{\overline{\Delta}}^2 \left|\hat{\overline{S}}\right| \hat{\overline{S}}_{ij} - 2\rho C_s \overline{\Delta}^2 \left|\hat{\overline{S}}\right| \hat{\overline{S}}_{ij} \tag{8}$$

A second order tensor similar to L_{ij} is definedby the above formula.

$$M_{ij} = 2\rho C_s \overline{\overline{\Delta}^2 \left|\hat{\overline{S}}\right| \hat{\overline{S}}_{ij}} - 2\rho C_s \hat{\overline{\Delta}}^2 \left|\hat{\overline{S}}\right| \hat{\overline{S}}_{ij} \tag{9}$$

So $\boldsymbol{L}_{ij}=C_s\boldsymbol{M}_{ij}$, then based on the least square method you can get

$$C_s = \boldsymbol{L}_{ij}\boldsymbol{M}_{ij} / \boldsymbol{M}_{kl}\boldsymbol{M}_{kl} \tag{10}$$

It can well predict the fully developed turbulent flow, and can be applied to the simulation of flow field around the cooling tower structure of high Reynolds number (Ke *et al.* 2013, Ke *et al.* 2015, Ke *et al.* 2015).

3.3 Boundary conditions and parameters

Velocity inlet and pressure-outlet are employed for computational domains in this study. The top surface and side were defined as Symmetry with free sliding capacity and the floor and structure surface were defined as Wall with no free sliding capacity. The fluctuating wind fields are defined using the UDF document, while the exponential wind profile of the atmospheric boundary layer and turbulence intensity profile of Level B landform were employed. The ground roughness of the wind profile was 0.15. Fig. 3 shows the practically measured average wind profile, turbulence intensity, and fluctuating wind spectrum of Level B fluid fields in numerical wind tunnels. As observed, the average wind profile obtained is consistent with standard ones. Meanwhile, the practically measured fluctuating wind spectrum were fitted and compared with the Davenport spectrum, the Harris spectrum, and the Karman spectrum. The results revealed that the fluctuating wind spectra obtained by the wind field simulation in this study are precise and accurate.

The 3D single precision separation solver was employed for numerical simulation and the atmosphere wind fields were defined as uncompressible ones. Coupling of pressure and velocity was achieved using the LES-based SIMPLEC algorithm, which is characterized by excellent convergence and suitability for LES simulations with small time steps. Grid tilt correction was involved to mitigate incompatibility of different meshes and the calculation residual of the controlling equation was defined as 1×10^{-6}. The time step was 0.05 s and 6000 steps were involved.

3.4 Model validation

As current standards (VGB-R 610Ue 2005, Blanchette *et al.* 2013, GB/T 50009-2012, GB/T 50102-2014) describe surface wind load distribution on constructed towers only, Fig. 4 compares average and fluctuating wind loads on typical cross section of the target tower with standards and results reported by previous studies. Two conclusions can be drawn. First, the results of average wind pressure distribution in the lower section are consistent with those of the standard curve. The wind pressure coefficient in the windward side is in good agreement with the value, and the negative pressure in the crosswind side and the leeward side is a little larger than the standard curve. The corresponding angles of maximum negative pressure and separation side on the surface of laryngeal section are consistent with the standard curve, and the wind pressure coefficient in windward side is in good agreement with the standard value. The numerical value of the crosswind side and the leeward side is slightly smaller than the standard value, and the relative error is not more than 5%. Second, the distribution of fluctuating wind pressure obtained by large eddy simulation is close to the measured curve abroad, and is smaller than that obtained from abroad. In fact, the distribution of fluctuating wind pressure is related to the topography of the measured tower, the turbulence of the incoming flow and the interference around the tower, and the distribution of fluctuating wind pressure measured at different heights is quite different.

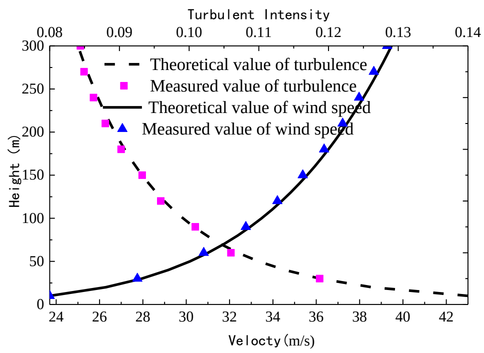

(a) Velocity and turbulence intensity

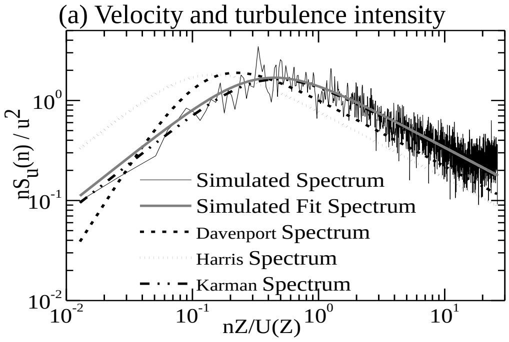

(b) Fluctuating wind load spectrum

Fig. 3 Velocity and turbulence profiles

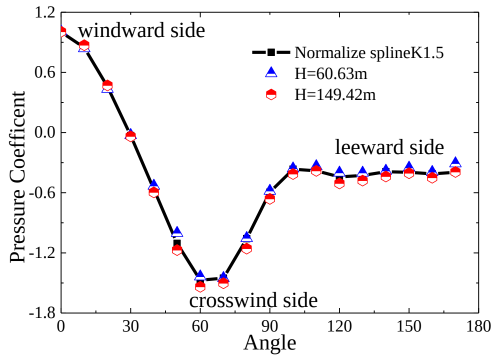

(a) Average wind pressure

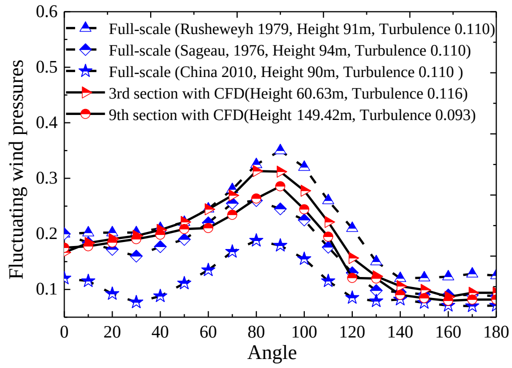

(b) Fluctuating wind pressure

Fig. 4 Wind pressures on typical cross sections obtained by numerical simulation and practical measurement

The wind pressure curve in China is obtained by measuring the upper throat position of a super large cooling tower in Xuzhou Power Plant in Fig. 4. The test height is high, so the fluctuating wind pressure coefficient is relatively small. Its test height is so high that the fluctuating wind pressure coefficient is relatively small. The trends and values of fluctuating wind pressure distribution obtained by the large eddy simulation are both in the existing experimental and experimental results envelope. Therefore, it is considered that the fluctuating wind pressure based on large eddy simulation is effective, and can be used for subsequent time-domain characteristic analysis of wind loads.

4. Average wind pressure

4.1 Distribution of average pressure coefficient

Fig. 5 shows surface pressure coefficient distribution on the tower under different construction conditions. As observed, pressures on the tailwind areas are positive while pressures on the crosswind and leeward areas are negative under all construction conditions. The distributions of average circumferential wind pressures were consistent with the standards under all construction conditions (especially Construction Condition F). Additionally, the shape of the positive pressure zone in the tailwind area evolved from a horizontal ellipse to a vertical ellipse as the construction

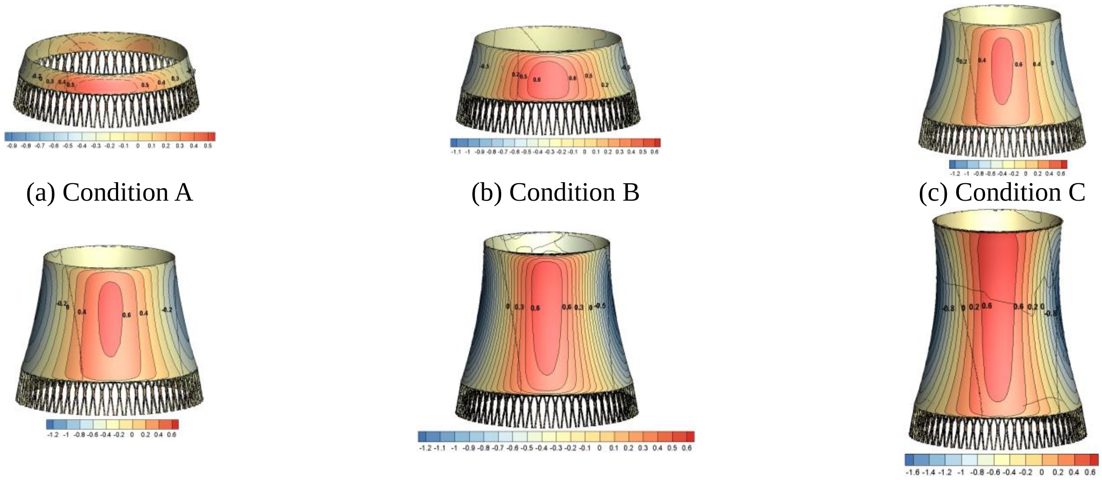

(a) Condition A (b) Condition B (c) Condition C

(d) Condition D (e) Condition E (f) Condition F

Fig. 5 Distributions of average pressure coefficient on the tower surface under different construction conditions

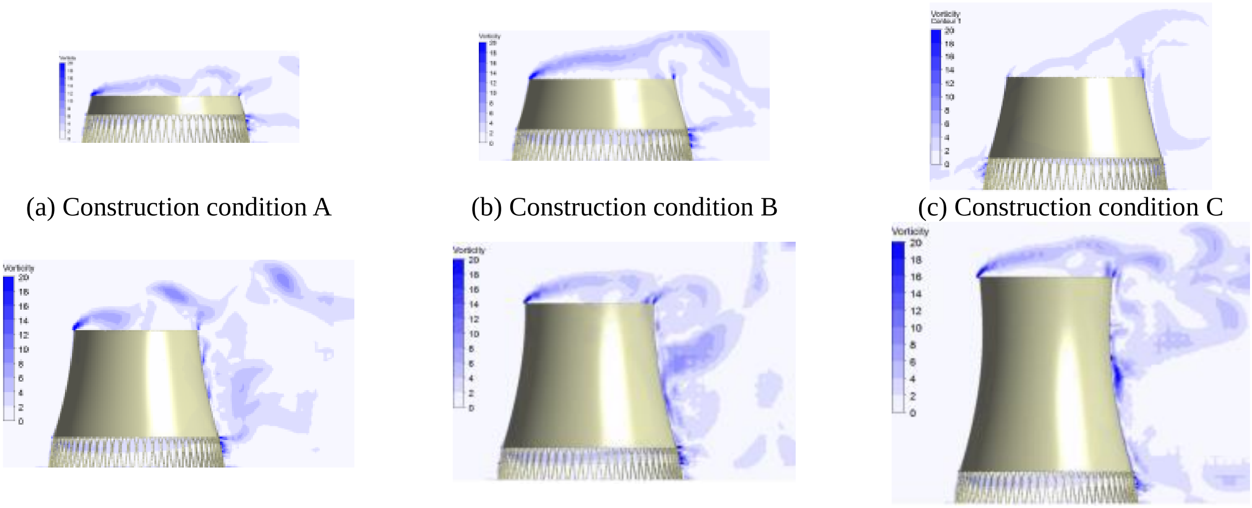

(a) Construction condition A (b) Construction condition B (c) Construction condition C

(d) Construction condition D (e) Construction condition E (f) Construction condition F

Fig. 6 Vorticities of x-z cross sections corresponding to different construction heights under different conditions

height increased. Meanwhile, the extreme negative pressure on the crosswind area and the average pressure coefficient increased with the construction height. The extreme positive pressure on the tailwind area increased from 0.5 to 0.6, while the extreme negative pressure on the tailwind area decreased from -1.1 to -1.4.

4.2 Principles of fluid fields

Fig. 6 shows vorticities of x-z cross sections corresponding todifferent construction conditions. As observed, the vortex distribution varied with the construction conditions. Significant vortex increasing zones were observed near the air outlet as the construction height increased, indicating significant vortex shedding as a result of increasing construction height. The vortex increasing zones in the leeward area were observed near the air inlet and the air outlet. Due to the increasing height, the pressure different between the air inlet and the air outlet, resulting in multiple eddies. Additionally, air flows from the air outlet and the lower part of the tower were separated as the construction height increased and significant bound eddies were observed in the negative pressure zone of the leeward area.

Table 2 presents velocity flow charts at typical construction heights under different construction conditions. As observed, the construction height has a significant effect on the initiation location of vortex shedding and wake development. More specifically, the wake development zone shrank and then expanded, while the increasing rate of wind speeds at tower sides increased as the construction height increased. Additionally, the construction height has an effect on air flow inside the tower, resulting in eddies in crosswind and leeward areas. Interactions of these eddies affected the location of flows in the leeward areas on the inner wall of the tower and the flowing direction shifted as the construction height increased.

Table 2 Velocity flow charts at typical construction heights under different construction conditions

Explain	Z=44 m	Z=70 m	Z=99 m	Z=129 m	Z=159 m	Z=202 m
ConditionA	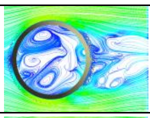					
ConditionB	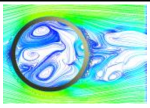	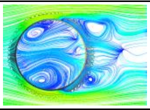				
ConditionC	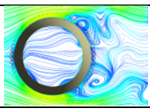	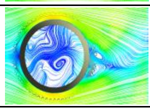	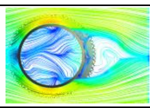			
ConditionD	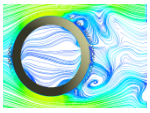	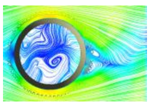	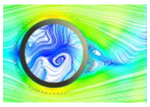	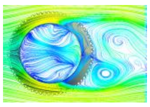		
ConditionE		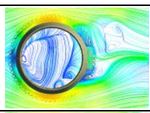	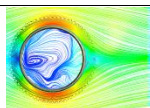	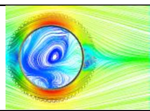	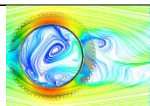	
ConditionF		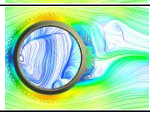	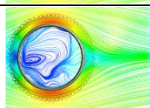	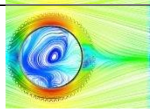	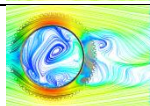	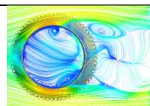

Table 3 Coefficients of target fitting formula

b_1	345.45	b_6	-1.45	b_{11}	7.57
b_2	-11.53	b_7	-5.13	b_{12}	-0.10
b_3	6.80	b_8	0.13	b_{13}	322
b_4	-0.17	b_9	-0.16	b_{14}	-10.67
b_5	23.32	b_{10}	0.80	b_{15}	1.00

5. Characteristics of fluctuating wind pressure time domain

5.1 Distribution of extreme wind pressure

The extreme wind pressure, which is a key indicator of structural stability of towers under construction, can be calculated using the following equation

$$\hat{C}_{pi} = \bar{C}_{pi} \pm g\sigma_{pi} \tag{11}$$

Where $\hat{C}_{pi}$, $\bar{C}_{pi}$, and σ_{pi} are the extreme value, the average value, and the root of variance of wind pressure coefficient of measuring point *i*. g, which is defined to be 2.5 in this study, is the peak value factor of measuring point *i*(GB/T 50009-2012).

Fig. 7 shows extreme wind pressure as a function of the construction height. As observed, trends of circumferential extreme wind pressure on typical cross sections under different construction conditions were consistent. As the construction height increased, negative pressure on a specific cross section varied significantly while the positive pressure on the tailwind area showed negligible variations. The existence of end effect makes the extreme value of negative pressure on the bottom and top of cooling tower vary greatly with the increase of height. The maximum extreme value of negative pressure are reduced to -3.91 and -2.28 from the original -1.36 and -1.29, respectively, while the extreme wind pressure in the central part of the tower was less affected by the construction height, from the initial -1.49 to -1.75.

Previous studies focused on extreme wind pressure distribution on constructed towers, while the 2D characteristics of extreme wind pressure distributions along circumferential and meridian directions on constructing ultra-large cooling towers were not taken into consideration. As a result, the extreme wind pressure distributions predicted showed significant differences from practically measured distributions. To avoid these errors, a fitting formula of extreme wind pressure as a function of meridian height and circumferential angle was proposed based on the nonlinear least square method

$$\begin{aligned} \boldsymbol{M}_{\theta,z} = {} & (b_1\boldsymbol{I} + b_2\boldsymbol{Z} + b_3\boldsymbol{Z}^{.2} + b_4\boldsymbol{\theta}\cdot\boldsymbol{Z} + b_5\boldsymbol{\theta}^{.3} \\ & + b_6\boldsymbol{Z}^{.3} + b_7\boldsymbol{\theta}^{.4} + b_8\boldsymbol{Z}^{.4} + b_9\boldsymbol{\theta}\cdot\boldsymbol{Z}^{.3} + b_{10}\boldsymbol{\theta}^{.2}\cdot\boldsymbol{Z}^{.2} \\ & + b_{11}\boldsymbol{\theta}^{.5} + b_{12}\boldsymbol{Z}^{.5}) \cdot\div (\boldsymbol{I} + b_{13}\exp(b_{14}\boldsymbol{\theta} + b_{15}\boldsymbol{Z})) \end{aligned} \tag{12}$$

Where the cooling tower is divided into n_1 and n_2 sections along circumferential and meridian directions ($N = n_1 \times n_2$), I is a A×1 matrix whose elements are 1,θ isa A×1 matrix that repeats n_2 times from n_1 angles, Z is a A×1 matrix that repeats n_1 times with n_2 identical heights. ·× refers to multiplication of corresponding elements in the

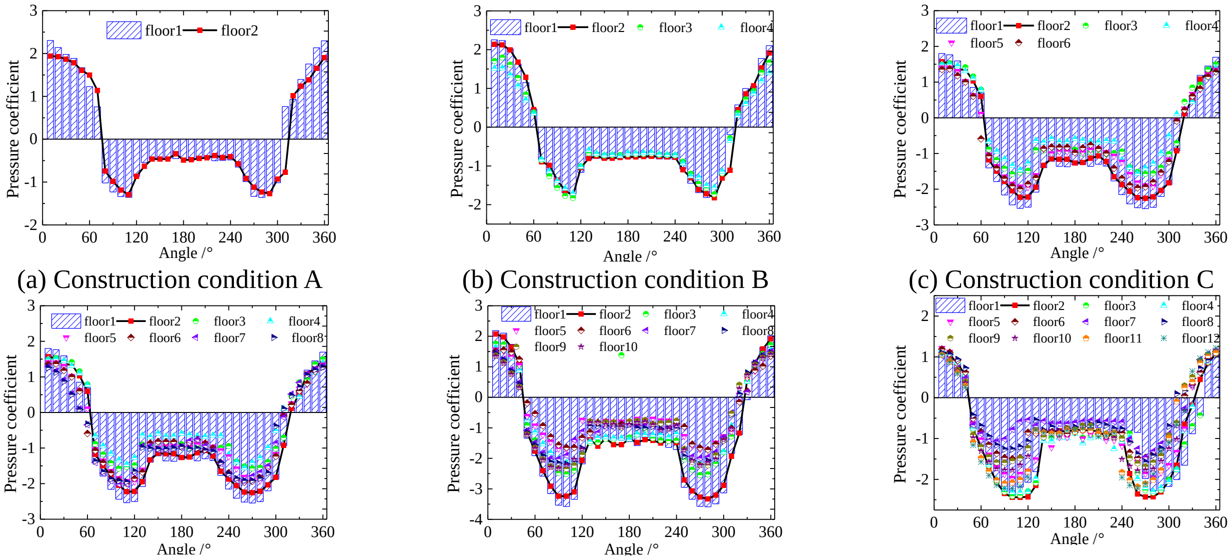

(a) Construction condition A (b) Construction condition B (c) Construction condition C

(d) Construction condition D (e) Construction condition E (f) Construction condition F

Fig. 7 Distributions of extreme wind pressure as a function under different construction conditions

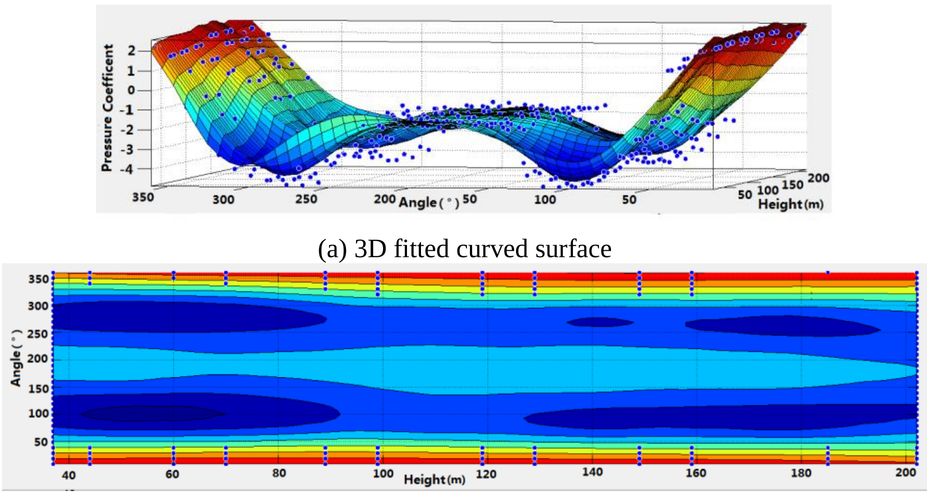

(a) 3D fitted curved surface

(b) Contour lines of fitted curved surface

Fig. 8 2D fitted curved surface of extreme wind pressure along the meridian height and the circumferential angle predicted by the 2D fitting formula and results practically measured

matrix, ·÷ refers to division of corresponding elements in the matrix, ·n refers to n times of corresponding elements in the matrix, exp() refers to a matrix containing exponential functions of each element in the initial matrix, $M_{\theta,Z}$ isa A×1 matrix with wind vibration coefficients corresponding to n_1 circumferential angles and n2 changes along the meridian height, b_i (i=1, 2,…,15) is the fitting coefficient (see Table 3).

Fig. 8 shows distribution and fitted curved surfaces of extreme wind pressure of ultra-large cooling towers along the construction height. Values of scatter points are practically measured extreme wind pressures and values on the curved surface are predicted by the 2D fitting formula proposed. As the construction height increased, the extreme wind pressure on the tailwind area increased while extreme wind pressure on the leeward area decreased and then increased (symmetric to the middle part of the tower).According to the distribution of the overall extreme wind pressure, the extreme wind pressure fitted with the height of the target is in good agreement with the true extreme wind pressure. The comparison results show that the extreme wind pressure fitting formula proposed in this paper can provide the basis for the calculation of extreme wind pressure in the construction period of such large cooling towers.

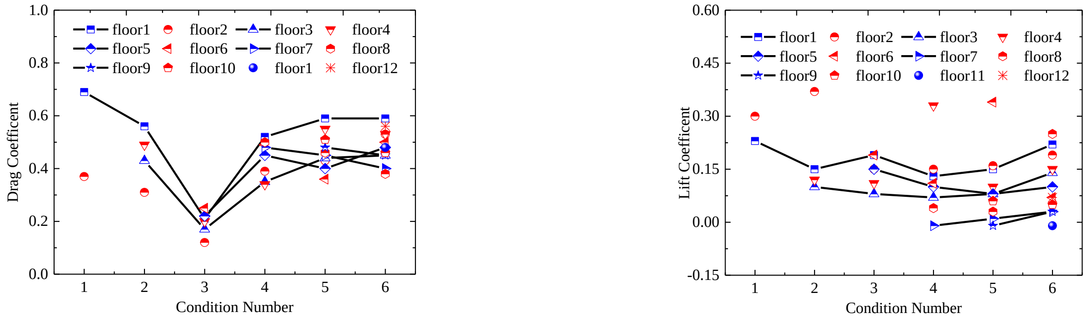

(a) Drag coefficient (b) Liftcoefficient

Fig. 9 Lift and drag coefficients as a function of the construction height under different construction conditions

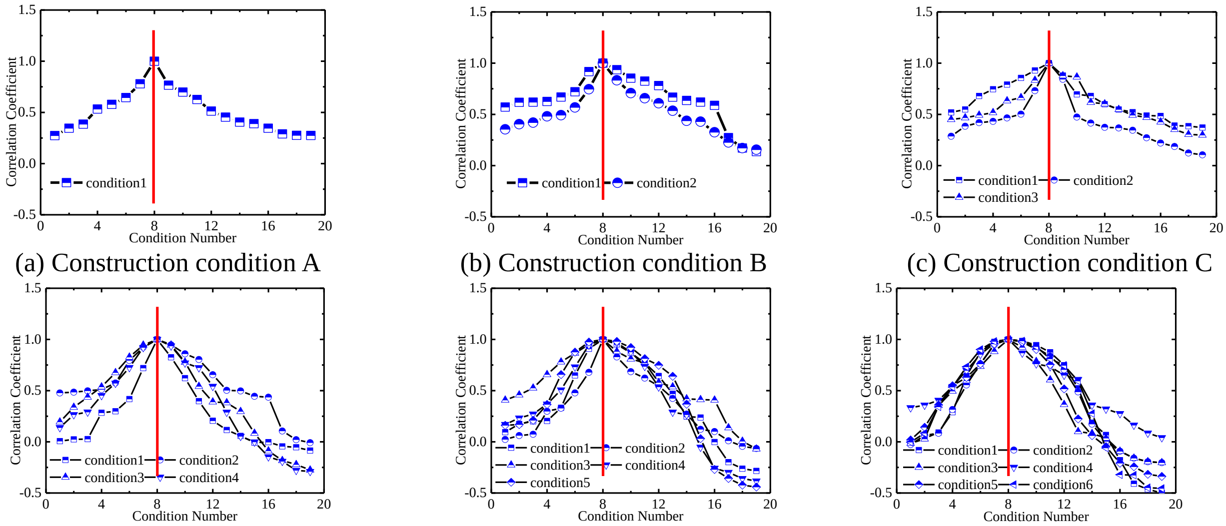

(a) Construction condition A (b) Construction condition B (c) Construction condition C

(d) Construction condition D (e) Construction condition E (f) Construction condition F

Fig. 10 Correlation distribution curves of extreme negative pressure measured at points on typical cross sections

5.2 Characteristics of lift and drag coefficient

To established a better understanding of mechanical performances of constructing cooling towers, the trends of lift and drag coefficients as a function of the construction height under different construction conditions were obtained and compared with each other. The lift and drag coefficients are defined as

$$C_D = \frac{\sum_{i=1}^{n} C_{Pi} A_i \cos(\theta_i)}{A_T} \tag{13}$$

$$C_L = \frac{\sum_{i=1}^{n} C_{Pi} A_i \sin(\theta_i)}{A_T} \tag{14}$$

Where C_D and C_L are the overall drag coefficient and the overall lift coefficient, respectively; A_i is the pressure area of the *i*th measuring point; θ_i is the angle between the pressure and the wind axial direction on the *i*th measuring point; A_T is the projected area of the overall structure in the wind axial direction.

Fig. 9 shows lift and drag coefficients at typical heights under different construction conditions. Owing to synergistic effects of inflow turbulence and vortex shedding on lift coefficients, trends of average lift coefficients along the construction height are significantly different from those of average drag coefficients. More specifically, the lift coefficient decreased while the drag coefficient decreased and then increased as the height increased. This is consistent with distributions of positive pressure on the tailwind area. Despite of construction conditions and location of measuring points, the lift coefficient was larger than the drag coefficient. The drag coefficient of each test point layer is larger than the lift coefficient under different working conditions. However, the decrease of the negative pressure on both sides of the tower leads to the increase of the lift coefficient and the decrease of the drag coefficient respectively. In addition, there is a phenomenon that the drag coefficient is less than the lift coefficient in the significant interference section in the middle of the tower under different working conditions.

Table 4 Coefficients table of target fitting formula

Fitting Coefficients					
b_1	0.9122	b_4	0.6914	b_7	-1.0610
b_2	-3.4970	b_5	-4.1560	b_8	0.1613
b_3	3.7990	b_6	3.1570		

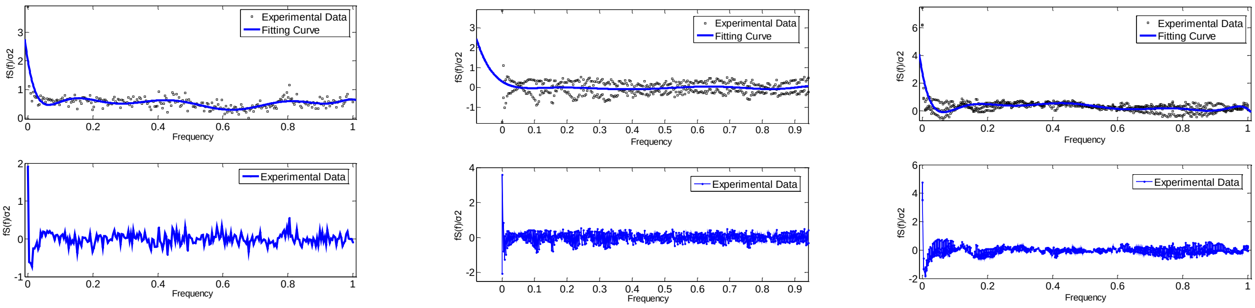

(a) Construction condition A (b) Construction condition B (c) Construction condition C

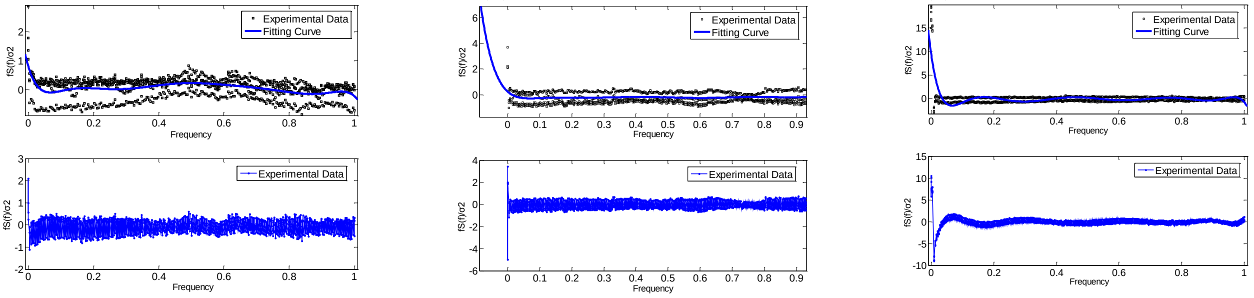

(d) Construction condition D (e) Construction condition E (f) Construction condition F

Fig. 11 Distribution curves of power spectra obtained by typical measuring points under different construction conditions

5.3 Correlation of fluctuating wind pressure

According to previous studies (Ke *et al*. 2015, Pirner1982), the extreme negative pressure on tower surface has a strong correlation to the separation points. Specifically, the extreme negative pressure on the crosswind area is negatively correlated to the separation points. Hence, effects of the construction height on the fluctuating wind pressure were investigated based on the extreme negative pressure zone. Fig. 10 shows correlation distribution curves of extreme negative pressure obtained by measuring points on the even floor and all circumferential measuring points under different construction conditions. Two conclusions can be drawn. First, the correlation in the middle part of the tower is significantly higher than correlations on bottom and top surfaces due to 3D end effect. Circumferential correlations increased and then decreased from Construction Condition A to Construction Condition F. Second, the construction conditions have a significant effect on the wind pressure. More specifically, correlations of Construction Conditions A, B, and C were highly consistent and higher than those of Construction Conditions D, E, and F. Under Construction Conditions A, B, and C, 2/3 of all measuring points were located in the strong correlation zone; under Construction Conditions D, E, and F, 1/3 of all measuring points were in the weak correlation zone as they exhibited significant negative correlation (up to 0.5).

6. Characteristics of fluctuating wind pressure frequency domain

6.1 Power spectra of typical measuring points

Fig. 11 shows scatter point distributions of dimensionless power spectra obtained by measuring points on the even floor under different construction conditions.

Equation for power spectrum density curve is as follows

$$f(x)=b_1x^7+b_2x^6+b_3x^5+b_4x^4+b_5x^3+b_6x^2+b_7x+b_8 \quad (15)$$

Where $f(x)$ is the power spectrum density as a function of wind pressure frequency and b_i (i=1, 2,…,15) is the fitting coefficient (see Table 4).

The fluctuating wind load energy concentrated in low frequency zone and separation points concentrated on bottom and top surfaces. This explains the fact that the wind fluctuating wind load energy decreased and then increased as the construction height increased. The fitting curves of power spectra under different construction conditions were significantly different. More specifically, peaks were observed in low frequency zones under Construction Conditions D, E, and F and the quantity of small peaks increased with the frequency; the low frequency zone under Construction Condition E exhibited maximized peak intensity and small peak quantity. Despite relatively high low frequency energy, multiple peaks in this case may be

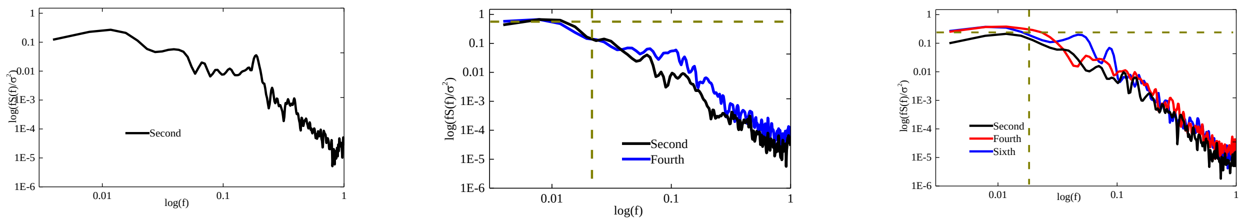

(a) Construction condition A (b) Construction condition B (c) Construction condition C

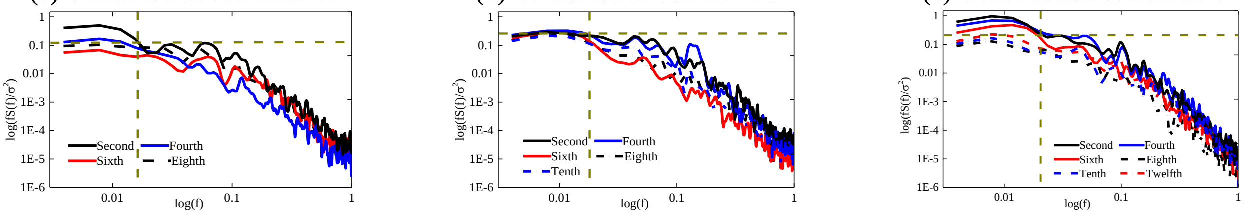

(d) Construction condition D (e) Construction condition E (f) Construction condition F

Fig.12 The power spectrum distribution curve of drag coefficient under different construction conditions

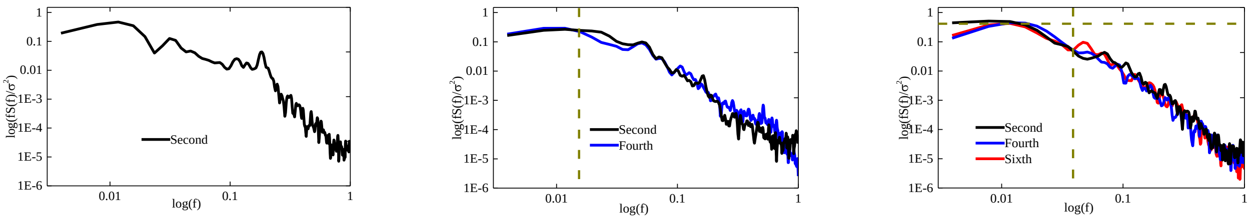

(a) Construction condition A (b) Construction condition B (c) Construction condition C

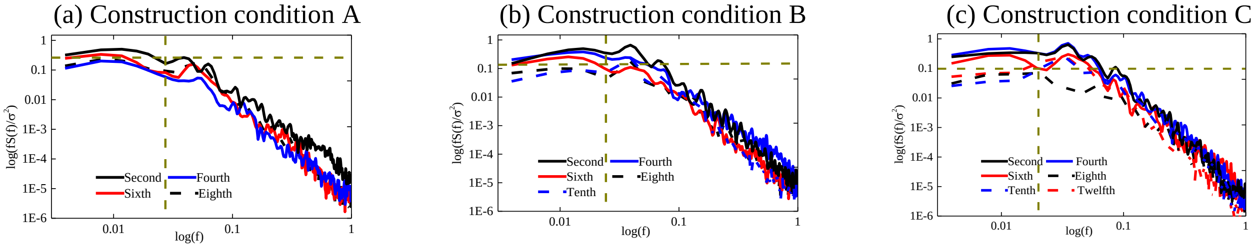

(d) Construction condition D (e) Construction condition E (f) Construction condition F

Fig. 13 The power spectrum distribution curve of lift coefficient under different construction conditions

attributed to airflow-induced separation bubbles and large scale, intermittent vortex shedding, which lead to energy increasing of power spectra at corresponding dominant frequency.

6.2 Power spectra of lift and drag

Figs. 12 and 13 show power spectrum distribution curve of drag and lift coefficient of typical cross sections, respectively. Two observations were made. First, the power spectra of drag coefficient decreased and then increased as the construction height increased, especially under Construction Conditions D and F; the power spectra of lift coefficient decreased as the construction height increased and significant separation was observed. Second, the low frequency bandwidth of the power spectra of drag coefficient decreased while the peak quantity increased as the construction height increased; in the high frequency zone, the power spectra of the middle part of the tower exhibited fast degradation, indicating relatively low fluctuating wind loads on this section. The power spectra of drag coefficient on the upper part of the tower exhibited relatively low values and the degradation rate in high frequency zone increased with the construction height.

6.3 Correlations between typical measuring points

Fig. 14 presents the function distribution curves of correlations between fluctuating wind pressures obtained by measuring points on the even floor at different construction heights, and fitting curve are given based on the formula (10). As observed, all curves are highly consistent and the correlations decreased and then increased as the frequency increased. The correlation function of fluctuating wind pressures obtained by measuring points in high frequency zone approached zero. Correlations of points in tailwind area and leeward area were significantly different and both degraded as the construction height increased. Additionally, the construction conditions have a significant effect on the correlation. The correlation was maximized under

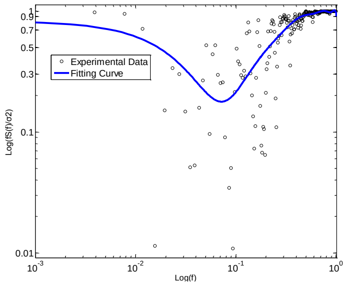

(a) Construction condition A

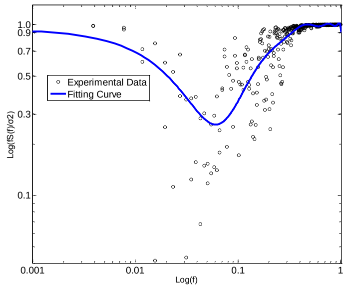

(b) Construction condition B

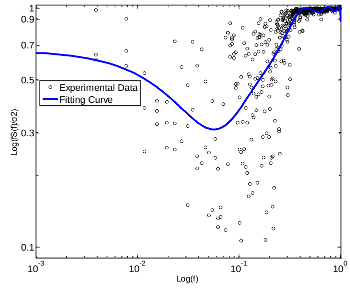

(c) Construction condition C

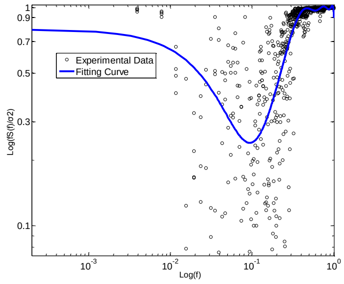

(d) Construction condition D

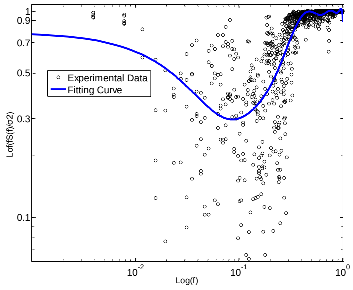

(e) Construction condition E

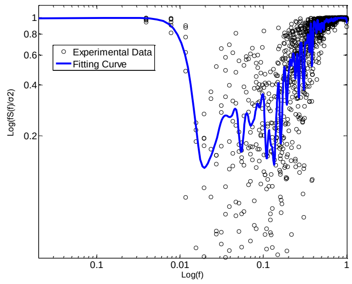

(f) Construction condition F

Fig. 14 Function distribution curves of correlations between fluctuating wind pressures obtained by measuring points on the even floor at different construction heights

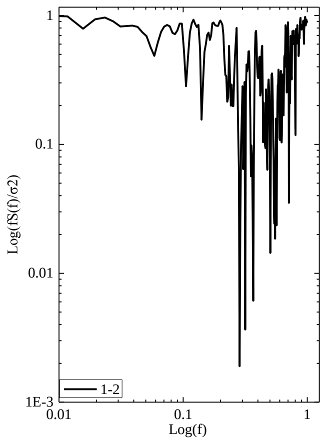

(a) Construction condition A

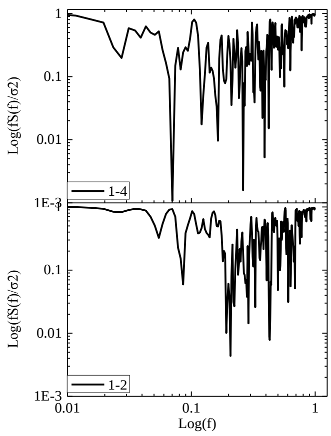

(b) Construction condition B

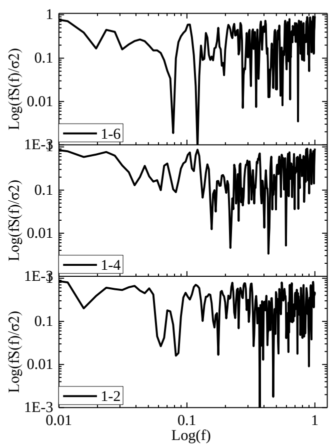

(c) Construction condition C

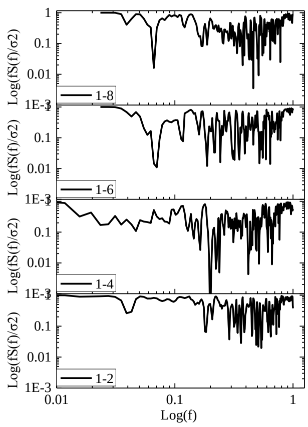

(d) Construction condition D

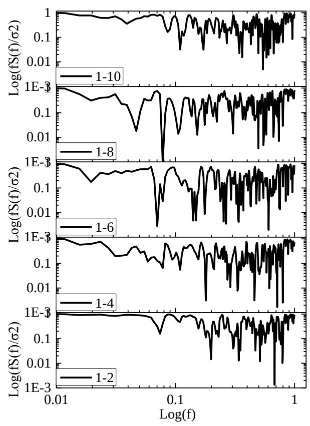

(e) Construction condition E

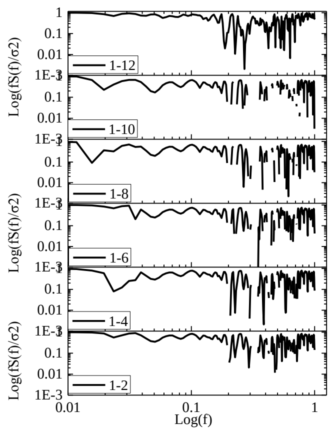

(f) Construction condition F

Fig. 15 Drag coefficients distribution curves of vertical correlation under different construction conditions

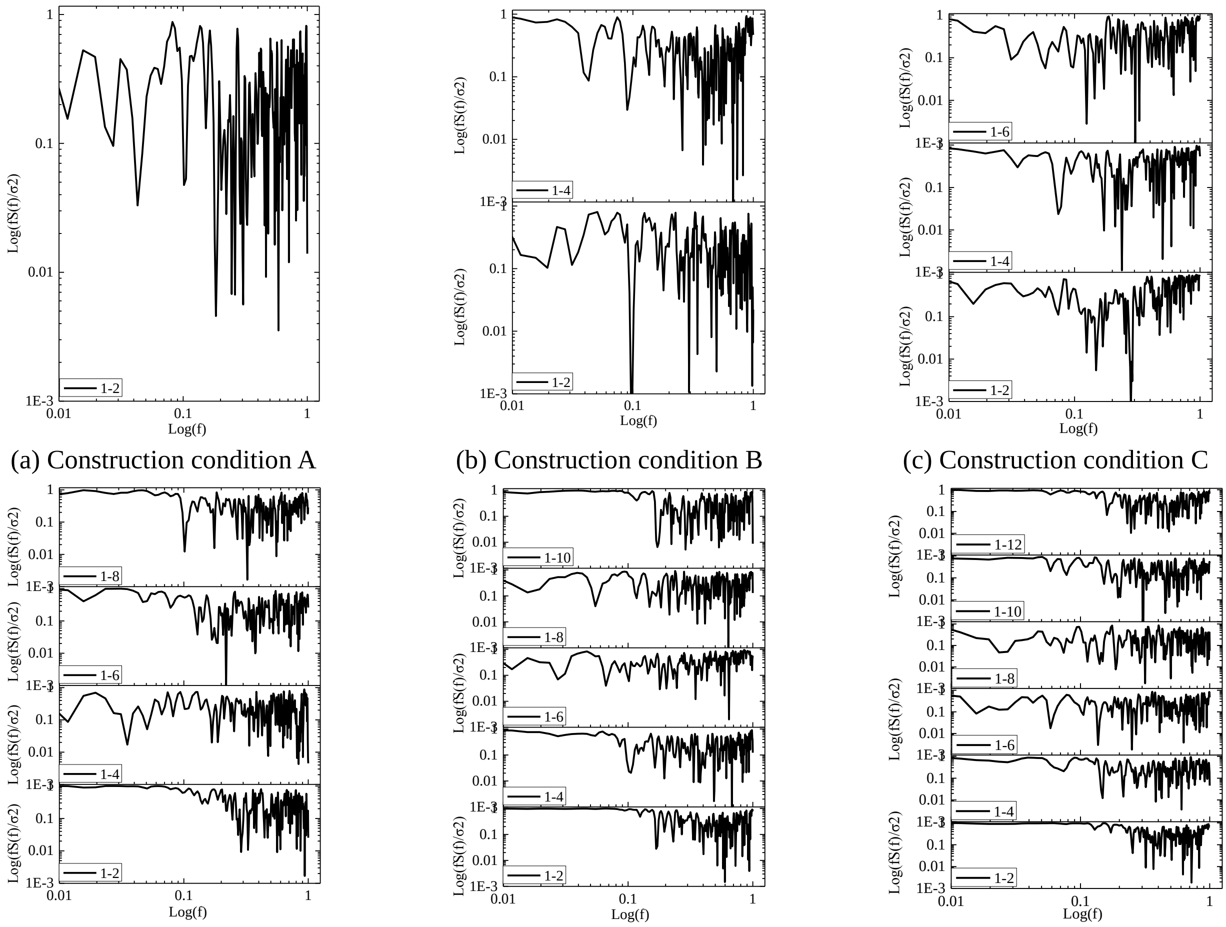

(a) Construction condition A (b) Construction condition B (c) Construction condition C

(d) Construction condition D (e) Construction condition E (f) Construction condition F

Fig. 16 Drag coefficients distribution curves of vertical correlation under different construction conditions

Construction Condition B and minimized under Construction Conditions E and F.

6.4 Vertical correlations of lift and drag coefficients

Figs. 15 and 16 show vertical correlation curves of lift and drag coefficients as a function of the construction height, respectively. As observed, vertical correlations of lift and drag coefficients decreased as the construction height increased under all construction conditions. The degradation rate in low frequency zone increased, while the increasing rate in high frequency zone decreased. As the fluctuating wind load energy concentrated in low frequency zone, the effects of fluctuating wind loads on the tower are significant at low construction heights. Additionally, the degradation rate of lift coefficient correlation in low frequency zone was significantly higher than that of drag coefficient correlation.

7. Conclusions

This study systematically investigates time domain and frequency domain characteristics of fluctuating wind loads on ultra-large cooling towers extreme in full construction process. The major focuses include LES, working principles of flow fields, extreme wind pressure, lift and drag coefficients, and correlation and extreme value fitting of fluctuating wind pressure power spectra. The following conclusions can be drawn:

- The shape of the positive pressure zone in the tailwind area of ultra-large cooling tower evolved from a horizontal ellipse to a vertical ellipse as the construction height increased, while the extreme negative pressure on the crosswind area increased continuously. Due to the increasing height, the pressure difference between the air inlet (lower part of the tower) and the air outlet (upper part of the tower) increased, resulting in multiple eddies. Additionally, accelerating flows in the velocity increasing zone on tower sides are strengthened and significant bound eddies were observed in the negative pressure zone of the leeward area.
- The circumferential correlations increased and then decreased under all construction conditions due to 3D end effect. The construction conditions have a significant effect on the wind pressure. Under Construction Conditions A, B, and C, 2/3 of all measuring points were located in the strong correlation zone; under Construction Conditions D,

E, and F, 1/3 of all measuring points were in the weak correlation zone as they exhibited significant negative correlation. As the construction height increased, the lift coefficient decreased while the drag coefficient decreased and then increased.

- As the construction height increased, the extreme wind pressures on the tailwind area increased, while the extreme wind pressures on the crosswind area decreased and then increased. Owing to the end effect, the effect of construction height on the tower was more significant in the middle part, compared with uppers and lower parts. A fitting formula of extreme wind load as a function of height was proposed based on the nonlinear least square method and this provides references for prediction of extreme wind pressures during construction of ultra-large cooling towers.
- The fluctuating wind load energy of both constructed and constructing towers concentrated in low frequency zone, while the fluctuating wind load energy in the middle part of the tower was relatively low. As the construction height increased, the fluctuating wind load and the density function of the power spectra of drag coefficient decreased and then increased. The power spectra of lift coefficient in the upper part of the tower were relatively low. Both the circumferential correlations of fluctuating wind loads and vertical correlations of lift and drag coefficients degraded as the construction height increased.

The results revealed that the time and frequency domains characteristics of fluctuating wind loads, as well as corresponding extreme wind pressure and power spectra curves, varied significantly and in real time with the height of the constructing tower. Main research findings provide references for design of wind loads during construction period of ultra-large cooling towers.

Acknowledgments

This project is jointly supported by National Natural Science Foundation (51208254 and 51021140005), Jiangsu Province Outstanding Natural Science Foundation (BK20160083), Jiangsu Qing Lan Project , Six talent peaks project in Jiangsu Province(JZ-026) and Postdoctoral Science Foundation (2013M530255; 1202006B), which are gratefully acknowledged.

References

Bao, K.Y., Shen, G.H. and Sun, B.N. (2010), “Hyperbolic cooling tower of fluctuating wind load simulation and wind-induced response”, *J. Zhejiang University (Engineering Science)*, **44**(5), 955-961. (In Chinese).

Binh, L.V., Ishihara, T. and Phuc, P.V. (2008), “A peak factor for non-Gaussian response analysis of wind turbine tower”, *J. Wind Eng. Ind. Aerod.*, **96**(10–11), 2217-2227.

Blanchette, J., Nelson, T.F. and Xuan, Z. (2013), “The British Standards Institution”, *Apha Meeting and Exposition*, 633-634.

Dauhut, T., Chaboureau, J.P. and Escobar, J. (2015), “Large-eddy simulations of Hector the convector making the stratosphere wetter”, *Atmosp. Sci. Lett.*, **16**(2), 135-140.

GB/T 50009-2012 (2012), “Load code for the design of building structures”, *The Ministry of Construction of China*, *Beijing*, *China*, 35-36.

GB/T 50102-2014 (2014), “Code for design of cooling for industrial recirculating water”, *The Ministry of Construction of China*, *Beijing*, *China*, 24-25.

Karakas, A.I., Ozgan, K. and Daloglu, A.T. (2016), “A parametric study for free vibration analysis of hyperbolic cooling towers on elastic foundation using consistent FEM-Vlasov model”, *Arch. Appl. Mech.*, **86**(5), 869-882.

Ke, S.T., Ge, Y.J. and Zhao, L. (2013), “Wind-induced responses of super-large cooling towers”, *J. Central South Univ.*, **20**(11), 3216-3228.

Ke, S.T. and Ge, Y.J. (2015), “Extreme wind pressures and non-Gaussian characteristics for super-large hyperbolic cooling towers considering aero-elastic effect”, *J. Eng. Mech*.. **141**(7), 04015010.

Ke, S.T., Wang, T.G., Ge, Y.J. and Yukio, T. (2015), “Stability and reinforcement analysis of super-large exhaust cooling towers based on a wind tunnel test”, *J. Struct. Eng.*, **141**(12), 04015066.

Kunitsu, H., et al. (2001), “Full-scale measurements of wind-induced vibration on Fukuoka tower: Part-3 Characteristics of fluctuating wind and pressures at the typhoons”, *Mar. Geology*, **178**(1), 39-62.

Li, P.F., Zhao, L. and Ge. Y.J. (2008), “Super large cooling tower wind load characteristics of wind tunnel test study”, *J. Eng. Mech.* (In Chinese), **25**(6), 60-67.(In Chinese).

Mang, H., Gallagher, R.H. and Cedolin, L. (2014), “Finite element instability analysis of Hyperbolic cooling tower”, *Adv. Civil Eng. Through Eng. Mech.*, 246-249.

Niemann, H.J., Harte, R., Meyer, J., et al. (2011) “Recent amendments to the VGB guideline on the design and construction of cooling towers in power plants”, *VGB Powertech*, **91**(9), 94-103.

Orlando, M. (2001), “Wind-induced correlation effects on two adjacent cooling towers”, *Eng. Struct.*, **23**(8), 979-992.

Pirner, M. (1982), “Wind pressure fluctuations on a cooling tower”, *J. Wind Eng. Ind. Aerod.*, **10**(3), 343-360.

VGB-R610Ue (2005), “VGB-Guideline: Structural design of cooling tower-technical guideline for the structural design, computation and execution of cooling tower”, *Essen: BTR Bautechnik BeiKühltürmen*.

Wang, W., Zhang, H., Liu, P., et al. (2017), “The cooling performance of a natural draft dry cooling tower under crosswind and an enclosure approach to cooling efficiency enhancement”, *Appl. Energ.*, **186**, 336-346.

Zhang, J.F., Ge, Y.J., Zhao, L., et al. (2017), “Wind induced dynamic responses on hyperbolic cooling tower shells and the equivalent static wind load”, *J. Wind Eng. Ind. Aerod.*, **169**, 280-289.

Zahlten, W. and Borri, C. (1998), “Time-domain simulation of the non-linear response of cooling tower shells subjected to stochastic wind loading”, *Eng. Struct.*, **20**(10), 881-889.

CC